

# Directionally solidified CeO<sub>2</sub> (or GDC)/CoO eutectic ceramics as cermet precursors for SOFCs anodes: Microstructure cross-over

Luis Ortega-San-Martin, José Ignacio Peña, Ángel Larrea, Victor M. Orera\*

*Instituto de Ciencia de Materiales de Aragón, CSIC-Universidad de Zaragoza, C/Maria de Luna 3, 50018 Zaragoza, Spain*

Received 15 December 2009; received in revised form 2 June 2010; accepted 30 June 2010

Available online 25 July 2010

## Abstract

Rods of CeO<sub>2</sub> and gadolinium-doped CeO<sub>2</sub> (GDC)–CoO eutectics were prepared by directional solidification using a laser heated floating zone (LFZ) technique. The microstructure has been studied as a function of the growth rate from  $V = 10$  to  $750$  mm/h. Regular eutectic microstructures are obtained except for the highest growth rate. The interspacing follows the  $\lambda^2 V = C$  law with  $C = 4.1(3) \times 10^{-17}$  and  $2.6(3) \times 10^{-17}$  m<sup>3</sup>/s for CeO<sub>2</sub>–CoO and GDC–CoO eutectics, respectively. A cross-over between fibrous and lamellar eutectic microstructures was observed depending on the growth rate. The crystallography of the eutectics was studied by Electron Backscatter Diffraction (EBSD). The growth directions  $[1\ 1\ 0]_{\text{GDC}} \sim // [1\ 1\ 0]_{\text{CoO}}$ , and the interfacial planes  $(200)_{\text{GDC}} // (111)_{\text{CoO}}$ , were identified. Solubility of Co in the ceria matrix was determined by Energy Dispersive X-ray (EDX) Spectroscopy after Co was leached out from the matrix. Co solubility in ceria at  $1650^\circ\text{C}$  was found to be less than 1 mol%. © 2010 Elsevier Ltd. All rights reserved.

**Keywords:** B. Composites; B. Microstructure-final; D. CeO<sub>2</sub>; E. Fuel cells; Eutectics

## 1. Introduction

Composites obtained by solidification of a melted binary eutectic mixture have been the subject of great interest since the middle of last century for their superior mechanical properties that may be used in the field of structural materials.<sup>1</sup> Initial studies were mostly confined to metal–metal eutectics but the extraordinary mechanical response and excellent thermal stability promoted thorough studies of the microstructure and crystallography of several Directionally Solidified Eutectic (DSE) oxides turned later the attention to oxide ceramic composites.<sup>2,3</sup>

The interest in this DSE oxides has not decreased with time, and eutectics have been proposed to be good candidates for use in several applications, namely optical, electronic, magnetic and in the energy production.<sup>4,5</sup> The unique microstructure of regular eutectics, made up of ordered arrays of alternating lamellae or fibres with sharp and clean interfaces, induces new functional properties, such as directional transport of light and improved ionic and electronic conductivity.<sup>6</sup>

The possibility of using eutectic ceramic oxides as precursor materials to obtain new composites, such as porous metal–ceramic mixtures has been successfully demonstrated by Revcolevschi and Dhalenne.<sup>7,8</sup> Metal–ceramic composites (cermets) containing an ionic conductor such as stabilised zirconia (or ceria) and a transition metal, such as Ni, Co or Cu, that are good catalysers of several chemical reactions, find applications in the fields of heterogeneous catalysis and in solid oxide fuel cell (SOFC) technology.<sup>9</sup> The continuous ionic conducting phase allows oxygen diffusion in and out the eutectic bulk; in this way reduction of the transition metal oxide phases inside the eutectic matrix is possible, making DSE oxides useful as precursor materials to obtain porous cermets.

SOFCs are foreseen as one of the cleanest and most efficient alternative energy sources to fossil fuel combustion in the near future.<sup>10,11</sup> The state of the art anode in SOFCs is a cermet of yttria stabilised zirconia (YSZ) with Ni particles. These cermets are usually synthesised via conventional solid state routes (raw oxides are mixed, fired and, after sintering, reduced under H<sub>2</sub>), which result in very fine ceramics but have the disadvantage of grain coalescence at Fuel Cell working temperatures (600–1000 °C).<sup>12</sup>

This deficiency of conventional cermets can be considerably minimised in cermets produced from DSE oxide precursors.

\* Corresponding author.

E-mail address: [orera@unizar.es](mailto:orera@unizar.es) (V.M. Orera).

Table 1  
compositions and growth rates applied to all the rods prepared.

Sample group	CeO <sub>2</sub> (mol%)	GDC (mol%)	CoO (mol%)	Growth rates (mm/h)
1	18	–	82	10, 100, 200, 500 and 750
2	–	18	82	
3	16.5	–	83.5	10, 200 and 750
4	18.5	–	81.5	

In fact reduction of the eutectic ceramic leads to channelled Ni(Co)–YSZ(GDC) porous cermets with alternating porous metal and ionic conductor lamellae that provide good electrical conductivity, gas permeation and a thermal expansion coefficient similar to that of the YSZ(GDC) ceramic scaffold. As a result the thermo-mechanical integration with other components in the SOFC is favoured.<sup>13</sup> In these materials the catalyser particles, of submicron size, are confined between the YSZ narrow lamellae.<sup>14</sup> The good adhesion through low-energy interfaces that is obtained in DSE cermets between the metal and the ceramic scaffold induces a great stability of the metallic particles against coarsening.<sup>15</sup>

In the present case, the fabrication of Co/ceria (or Gd doped ceria) oxide composites by the laser floating zone (LFZ) technique is investigated in order to evaluate their suitability as cermet precursors for SOFC anodes. The idea of using ceria phases instead of YSZ is due in part to the higher ionic conductivity of ceria vs. YSZ when working at low operation temperatures.<sup>16</sup> In addition, ceria is an excellent catalyser. Lowering the working temperatures is for low cost and high efficient SOFC technology. The eutectic microstructure of the Co/ceria (or Gd doped ceria) oxides has been microscopically characterised. The influence of the composition and solidification parameters in the microstructure of the composites grown at different rates by the LFZ method has been also studied.

## 2. Experimental

Rods of CeO<sub>2</sub> (and GDC):CoO eutectic compositions were grown with a CO<sub>2</sub> laser ( $\lambda = 10.6 \mu\text{m}$ ; Blade600, Electronic Engineering, Firenze) using a LFZ system following the same procedures detailed in previous studies.<sup>17</sup> The precursors for the rods were prepared from CeO<sub>2</sub> (99.9%, Aldrich) or 10% Gd doped CeO<sub>2</sub> (GDC) obtained from inorganic salt precursors as described by Gil et al.<sup>18</sup> and CoO (98% + 2% Co<sub>3</sub>O<sub>4</sub>, prepared from Co<sub>3</sub>O<sub>4</sub> 99.7%, Alfa Aesar) powders. The starting oxides were mixed in the desired composition in an agate mortar and the obtained powder was isostatically pressed for 4 min at 200 MPa and sintered for 4 h at 1350 °C. Four different compositions, given in Table 1, were prepared in order to fully characterise the eutectic point of this system and the associated microstructure. The eutectic composition CeO<sub>2</sub>(or GDC):CoO with a molar ratio of 18:82 used for samples 1 and 2 was originally proposed by Chen et al. for the CeO<sub>2</sub>/CoO eutectic.<sup>19</sup>

Rods approximately 2.5 mm in diameter were grown in air in two steps, first a downward pulling (densification) and later an upward growth. Different growth rates from 10 to 750 mm/h (see Table 1) were applied. Identical seed and feed pulling rate with-

out diameter reduction was used in all the cases except for growth rates of 750 mm/h for which the rod diameter was reduced to one half of the initial size. The rotation speed of the source rod and/or the grown eutectic rod in the initial step was fixed to 50 rpm in counter rotation but in the final step no rotation was used. The length of the molten zone was maintained at about 1.5 times the rod diameter. A polycrystalline seed rod was used to initiate the growth.

Microstructures were observed from polished transverse and longitudinal cross-sections of the grown rods using a scanning electron microscope (SEM, model 6400, Jeol, Tokyo, Japan) equipped with an INCA300 energy dispersive spectroscopy (EDS) system (Oxford Instruments). Computer analysis of SEM images was used to estimate the volume fraction of phases and interlamellar spacing.

The orientation relationships between the different phases of the resulting eutectic microstructures in the CeO<sub>2</sub>:CoO system at different growth rates were studied by electron backscattered diffraction (EBSD) using an Oxford Instruments HKL EBSD system attached to the SEM described before.

## 3. Results

Electron micrographs taken on transversal cross-sections at the rod's centre showing the microstructures of the samples with eutectic composition (groups 1 and 2) are presented in Fig. 1. Most samples show a fully aligned regular eutectic microstructure, either fibrous or lamellar, arranged in eutectic grains that are composed of ceria (or GDC) as the second phase (light) in a cobalt oxide matrix (dark). At 750 mm/h there is some tendency to form a colony type structure, which is more evident in the gadolinium-doped ceria eutectic (Fig. 2). Tendency to form colonies at high growth rates, *i.e.* high under-cooling rates, is typical in eutectic growth and is consistent with the constitutional under-cooling effect associated with high solidification rates that provoke a non planar growth front.<sup>1,20</sup> Constitutional under-cooling is sometimes attributed to the presence of impurities, but none were observed in the present study. The addition of Gd may have slightly altered the CoO:CeO<sub>2</sub> eutectic point and this small deviation could be the origin of instabilities in the growth, particularly at high growth rates, which would explain the observed result. The same tendency to form colonies of similar morphology was observed by Sayir and Farmer when a third component, Y<sub>2</sub>O<sub>3</sub>, was added to the binary Al<sub>2</sub>O<sub>3</sub>/ZrO<sub>2</sub> eutectic, confirming that small changes in composition can produce some modifications in the microstructure.<sup>21</sup> In any case, the microstructure inside colonies is quite regular and is lamellar.

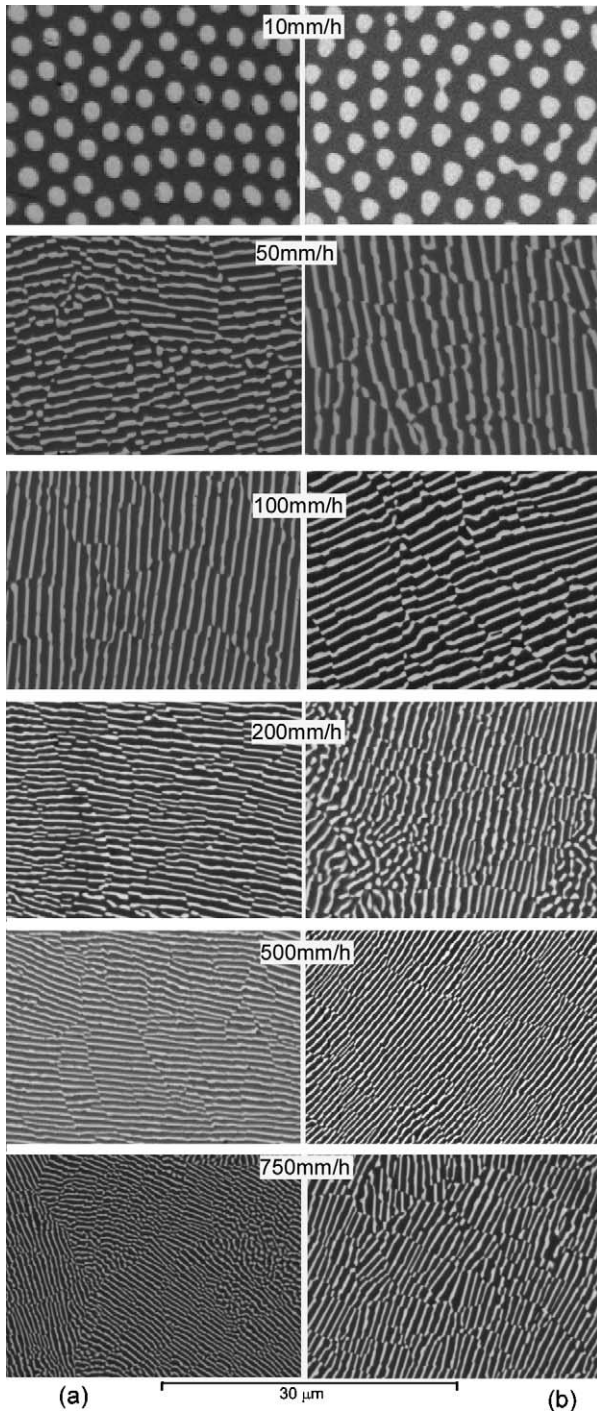


Fig. 1. SEM images of transverse rod sections showing the growth rate dependence of the eutectic microstructure of the sample groups 1 ( $\text{CeO}_2\text{:CoO}$  eutectic) and 2 ( $\text{GDC:CoO}$  eutectic). Micrographs taken at 20 kV in backscattered mode.

Regular eutectic microstructures are usually characterised by the dependence of the interlamellar (or inter-rod) spacing,  $\lambda$ , with the growth rate,<sup>22</sup> which can be intuitively seen in Fig. 1. For a flat, uniform advancing solid–liquid interface this dependence follows the law proposed by Hunt and Jackson<sup>23</sup>:

$$\lambda^2 V = C \quad (1)$$

where  $C$  is a constant and  $V$  is the growth rate. According to this law,  $\lambda$  should follow a linear behaviour with the

inverse of the square of the growth rate. Fig. 3 shows the inter-spacing, measured from transverse rod sections, as a function of the growth rate. The two systems studied follow this law reasonably well, with deviations at high growth rates. Similar deviations have been previously reported in other eutectic systems.<sup>24,25</sup> This is because at high growth rates the eutectic Péclet number is not longer  $<1$  and the Hunt and Jackson law is not valid. The constants obtained from the fits are  $4.1(3) \times 10^{-17}$  and  $2.6(3) \times 10^{-17} \text{ m}^3/\text{s}$  for systems 1 ( $\text{CeO}_2$ ) and 2 ( $\text{GDC}$ ) of Table 1, respectively. This behaviour is very relevant for the possible application of these mixtures as precursors for cermets because the size of the final metallic particles and pores in the cermets would be strongly dependent on the growth rate.

Of great interest is also the change of the microstructure type with the growth rate. As shown in Fig. 1 there is a microstructure change from a well defined fibrous microstructure at 10 mm/h (with some marginal fibres, not shown) to a lamellar one at higher growth rates. Together with this cross-over there is also a change in the volume fractions of the two oxides present in each system. These volume relations were experimentally determined in two different regions of the rods from image analyses and are shown in Fig. 4. It is observed that at low growth rates the interiors of the rods are slightly depleted in ceria (or GDC) favouring the fibrous microstructure, whereas at high growth rates the volume ratios get richer in ceria, favouring a lamellar growth. This compositional change is surprising given that the starting composition in all cases has been the same, and is an interesting phenomena not observed elsewhere as will be discussed below.

To check if changes in the interfacial planes and/or growth directions could be in the origin of the fibrous to lamellar transition, EBSD experiments were performed on sample with both types of microstructures. Several areas of  $\text{CoO-GDC}$  samples grown at 10 mm/h (mostly composed of fibres) and 200 mm/h (lamellar) were investigated. In the 10 mm/h sample one marginal lamellar-like region was also studied together with the overall rod-like microstructure. In all the cases the same orientation relationship was observed. The growth directions were  $[1\ 1\ 0]_{\text{GDC}} \sim // [1\ 1\ 0]_{\text{CoO}}$ , and the interfacial planes  $(200)_{\text{GDC}} // (1\ 1\ 1)_{\text{CoO}}$ . Fig. 5 shows an EBSD orientation map and the associated pole figures of a fibrous region of the sample grown at 10 mm/h displaying this orientation relationship. This is the same orientation relationship as previously reported for the  $\text{NiO-YSZ DSE}$ .<sup>15,26</sup>

The ceria matrix was also characterised in order to establish the possible presence of dissolved cobalt in the  $\text{CeO}_2$  (and GDC) oxides at the eutectic temperature ( $\sim 1650^\circ\text{C}$ ), as it has been proposed in other studies.<sup>19</sup> To perform this study the grown eutectics were reduced under a 5%  $\text{H}_2/\text{Ar}$  reducing atmosphere, as described elsewhere.<sup>27</sup> The completion of the reduction process was determined by gravimetric analysis. The resulting cermets,  $\text{CeO}_2\text{:Co}$  and  $\text{GDC:Co}$ , were subsequently immersed into a diluted  $\text{HNO}_3$  ( $\sim 2\text{ M}$ ) solution at room temperature under slow agitation for 24 h. This procedure eliminated all metallic cobalt between the ceria lamellae, leaving a pure ceria matrix as shown in Fig. 6. EDX analysis of the emptied matrices in the SEM showed that, within the detection limits



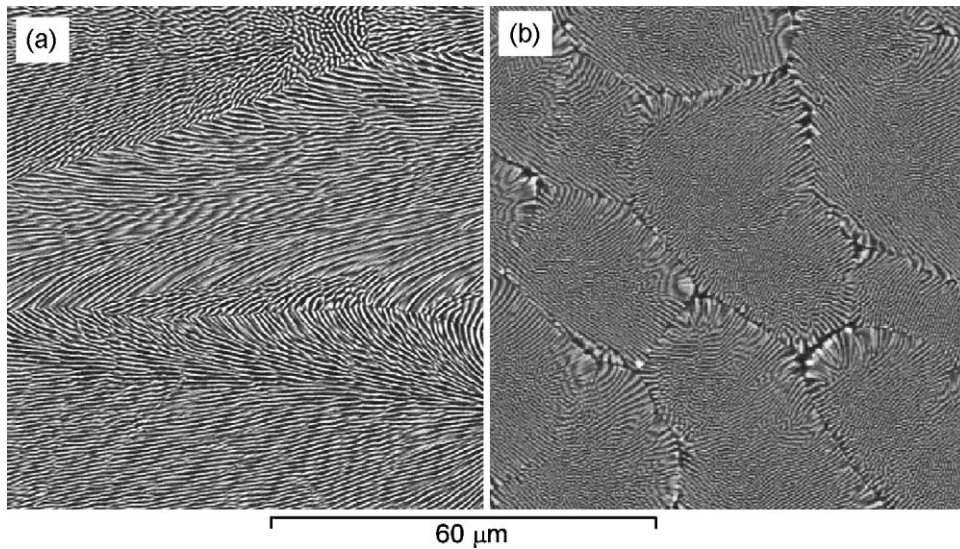


Fig. 2. SEM images showing longitudinal (a) and transverse section (b) views of the colonies in the GDC materials grown at 750 mm/h. Light phase is GDC and dark phase is CoO.

(less than  $\sim 1$  mol% of CoO), no cobalt was dissolved in the matrix. The same results were found on the rod precursors sintered at  $1350^\circ\text{C}$ . These are relevant results which contrast with previously published phase diagram<sup>19</sup> and are also important for the full characterisation of this system, the correct assignment of the phase diagram, and for the physicochemical properties of the ceria phase.

#### 4. Discussion and conclusions

The microstructure and composition of ceramic composites play a crucial role in determining their suitability for specific

applications. In the present case, to prepare suitable precursors for SOFC cermet it is necessary to take into account the required cermet specifications. In general SOFC cermets must present good gas permeation and excellent electronic and ionic conductivity through the metal and ceramic parts, respectively. To achieve this, both phases must be homogeneously distributed over the cermet with each component as small as possible, in order to increase the triple phase boundary (TPB) length, *i.e.* where the electrochemical reaction takes place. Good connectivity between the ceramic, the metallic particles and pores is also mandatory to ensure good electronic conductivity and gas permeation, respectively.<sup>11</sup>

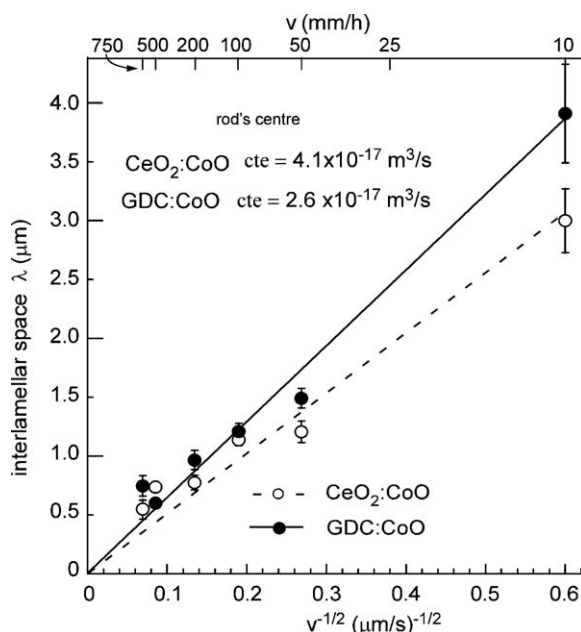


Fig. 3. Growth rate (as  $1/V^2$ ) dependence of the interlamellar ( $\lambda$ ) space in the CeO<sub>2</sub>:CoO and GDC:CoO systems. The interlamellar/interfibre spacing,  $\lambda$ , has been calculated in the centre of all rods, as indicated in the main text.

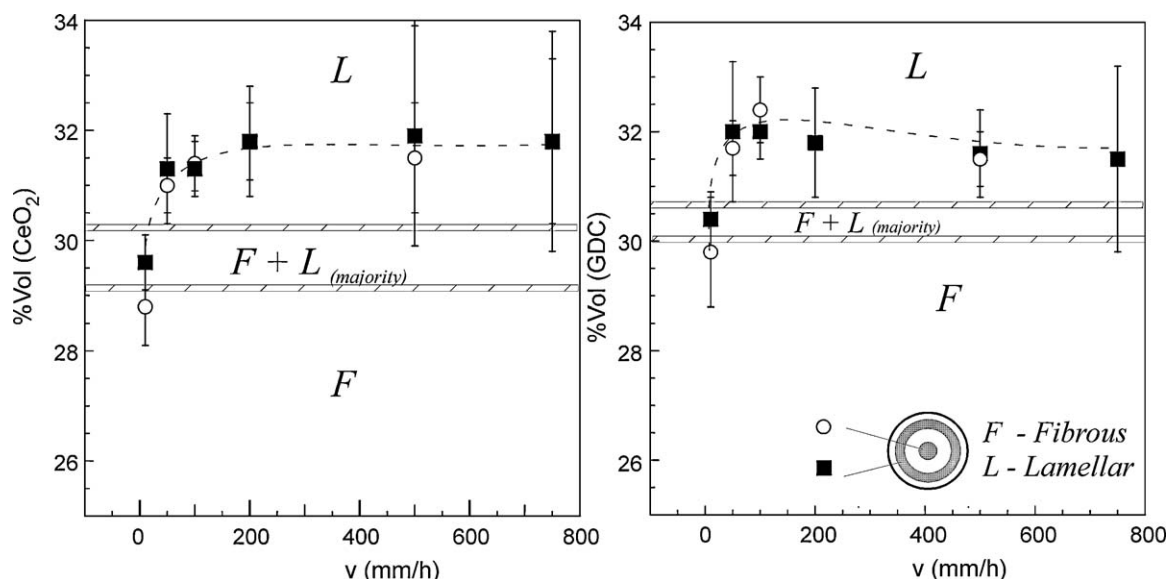


Fig. 4. Growth rate dependence of the CeO<sub>2</sub> (and GDC) volume percentage measured by image analysis at two different rod locations: the center (white circles) and the middle (black squares). Fibrous and lamellar regions are indicated. Lines are guides to the eyes.

The processing of the CeO<sub>2</sub> (or GDC)–CoO eutectic mixtures at different growth rates by the LFZ technique has allowed us to determine that the highest growth rate used (750 mm/h) is, within all the growth rates used, an appropriate rate to obtain a regular and very fine microstructure that will assure connectivity between phases together with good ionic and electronic conductivities of each component when the cermet is formed. The observed interlamellar spacing ( $\lambda$ ) is in the range of 0.5–0.7  $\mu\text{m}$  in both doped and undoped ceria phases, with the doped phases usually showing larger  $\lambda$ . These microstructural scales correspond to lamellae as thin as 150 nm (with a mean of  $\sim 200$  nm) in the case of ceria, and a thickness of 300 nm (with a mean of  $\sim 400$  nm) for the cobalt oxide counterpart. This very fine microstructure would result in a large number of TPBs following reduction. The detailed fabrication process of the cermets with the 750 mm/h samples and their microstructure characterisation and reduction kinetics have been presented elsewhere.<sup>27</sup>

The high degree of process control that can be achieved by the use of the LFZ technique has also allowed us to follow

the changes in the microstructure with the growth rate. In the present case two different microstructures have been observed depending on the growth rate.

Early studies in eutectic alloy systems indicated that rod-type structures would be formed due to the presence of impurities and as a result of the changes in the solid–liquid temperature gradient emerging from the presence of those impurities.<sup>28</sup> Later, another idea based on geometrical considerations gained position: in this case the appearance of a given microstructure, fibrous or lamellar, was associated with the minimisation of the interfacial surface during the formation of the eutectic microstructure. Accordingly, if geometrical considerations are taken into account and an isotropic surface energy is assumed during growth conditions, an array of fibres is favoured when the volume percent of one of the phases is less than 28–30% (a square array of fibres extends the transition to 32%).<sup>29</sup> Otherwise, the eutectic microstructure is generally lamellar.

This behaviour is followed by most oxide or alloy eutectics studied in the literature. However, some exceptions occur mainly when compositions are near the cross-over region. There

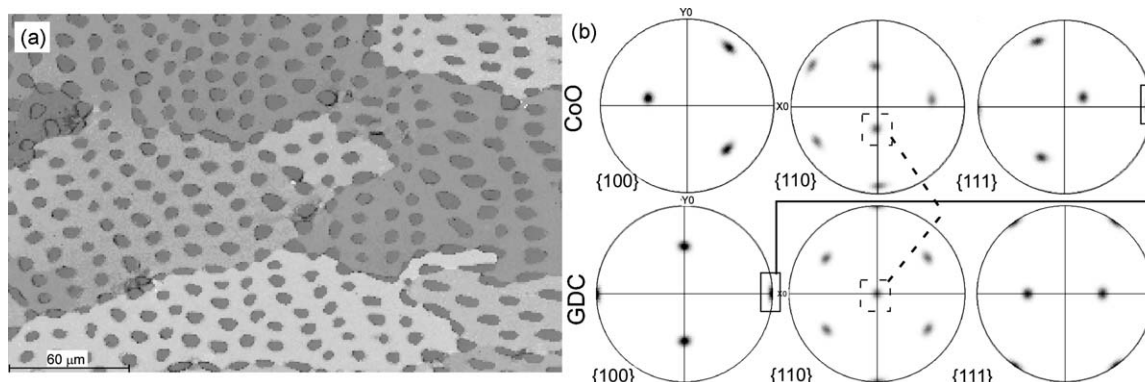


Fig. 5. EBSD orientation map showing the different eutectic grains (a) and associated pole figures (b) of a fibrous region of the rod grown at 10 mm/h. Dashed line in (b) links the growth directions and continuous line links interfacial planes.

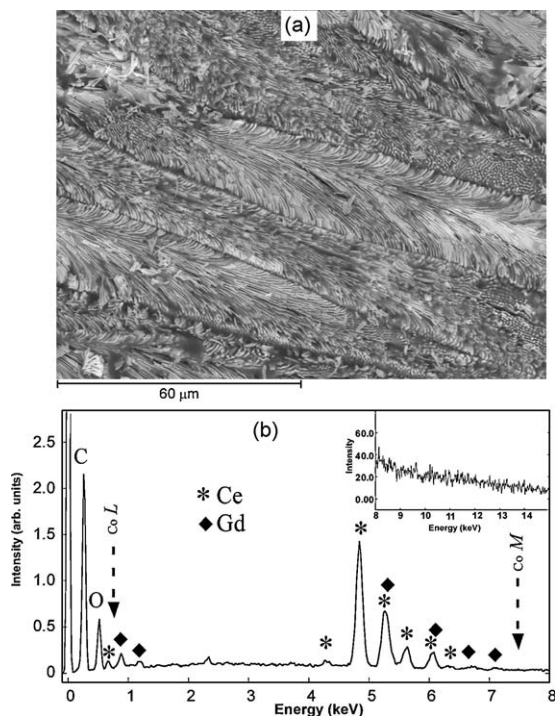


Fig. 6. (a) Electron micrograph of GDC matrix after reduction and elimination of the CoO oxide. The well organised lamellar microstructure can be clearly seen. Sample grown at 750 mm/h. (b) Typical EDS spectrum taken on a  $60 \times 60 \mu\text{m}$  region of the image shown in (a). Arrows indicate the absent cobalt K and L lines. Inset shows the high keV region with no peaks. Electrons accelerated at 20 keV, polished sample. Collection time  $\sim 750$  s.

are also exceptions that do not fall into the previous group, such as in the cases of Al–CuAl<sub>2</sub> and Cu–Sn<sup>30</sup> alloys, where lamellar structure is generally observed (and expected) but rod-like microstructures can be formed at high growth rates or if small amounts of impurities are introduced in the systems. In alloys, it is usually agreed that this intentional addition of impurities is responsible of the appearance of fibres due to the changes caused in the growth conditions (such as the appearance of under-cooled regions, inhomogeneous mixtures, etc.). In undoped systems and in oxides the lamellar–fibre transition has been proposed to occur whenever the new growth direction is not contained in the low-energy lamellar plane (at the boundaries of colonies), or due to non equilibrium solidification conditions.<sup>29</sup> This is the case of the Al<sub>2</sub>O<sub>3</sub>–ZrO<sub>2</sub> system, with compositions in the cross-over region, that has been shown to form lamellar microstructures under controlled low growth rates but mixtures of rod and lamellar-like microstructures (colonies at high rates) under not well controlled conditions and colonies under high growth rates.<sup>31</sup>

In the two eutectic systems under study (doped/undoped ceria–CoO) the starting compositions are nearly the same, and nominally  $\sim 31:69$  in volume % (see Table 1). According to these values both systems should be either in the lamellar region or near the cross-over fibrous/lamellar boundary. Our observations show a stepwise change from rod-like to lamellar microstructure instead of a mixed morphology as the growth rate increases. This change is also associated with an increase in the ceria volume fraction in such a way that it perfectly follows the geometry-

based theory (Fig. 4): measured volume fractions correlate well with either the fibrous or the lamellar regions as predicted.

This is a very interesting observation because in all cases the starting composition of the eutectic was exactly the same. Changes in the volume fraction, and in the type of eutectic microstructure, could be expected if any of the components are lost during growth. However, in the present case only CoO is suspected to be lost during growth conditions (the growth chamber shows some Co contamination) and the expected consequence of this loss would be an increase of the volume ratio of CeO<sub>2</sub> (or GDC) to CoO and hence a stabilisation of the lamellar microstructure in all samples.

However, this is not the case. Observations indicate that samples grown at 10 mm/h show a segregation of the ceria phase towards the border of the rods creating an outer CeO<sub>2</sub>/GDC dense layer of about 20  $\mu\text{m}$  thickness. Then about 3.2 vol% of the rod volume is made of ceria. This leaves a  $\sim 28.8$  vol% of CeO<sub>2</sub>/GDC inside the rod which coincides with the measured volume fractions of Fig. 4 and clearly corresponds to an eutectic fibrous microstructure.

In order to check if the microstructural morphology could be adjusted by small changes in compositions, two new sets of samples with slightly off-eutectic compositions were prepared: systems 3 and 4 of Table 1. Samples 3 and 4 were prepared considering the compositions obtained from the rods grown at 10 (fibrous) and 750 mm/h (lamellar), respectively. They were grown at three different growth rates and the results reproduced the observations already described for the eutectic system (Fig. 7): at 10 mm/h both show dominant fibrous structures whereas at higher rates they are completely lamellar. It is observed that the samples richer in ceria show a thicker external CeO<sub>2</sub> layer when grown at 10 mm/h thus favouring again the rod-like growth.

Similar trends observed in all the samples indicate that the eutectic composition can self-adapt to the growth conditions and find the preferred microstructural arrangement according to the growth rate. As shown by the EBSD studies on the samples, this change in the microstructure has no relation to the crystallographic orientation of the grains or the tendency to grow in a preferred orientation depending on the growth speed: there are no differences between the lamellar and rod configurations.

The CeO<sub>2</sub>/GDC layer is not observed at higher growth rates indicating that a segregation of CeO<sub>2</sub>/GDC in the liquid phase similar to that recently found in YSZ–NiO solidified eutectics may also take place in the present case.<sup>32</sup>

The change of microstructure with the growth rate is poorly documented and, in the few systems where some changes have been observed, the results are contradictory. In the oxide system MgO–MgAl<sub>2</sub>O<sub>4</sub>,<sup>29,33</sup> and in the alloy systems Al–Al<sub>4</sub>Ce and Al–Al<sub>3</sub>Y,<sup>34</sup> the change was the inverse: a lamellar to fibrous microstructure change is observed with increasing the growth rates. On the other hand, in Bi–Cd alloy<sup>35</sup> a degradation of the lamellar microstructure to a degenerated rod-like one has been reported when growth rates are very low (0.18 mm/h). In Ni–W alloys<sup>36</sup> a transition from localised grains with fibrous microstructure to lamellar microstructure was observed with increasing growth rate.



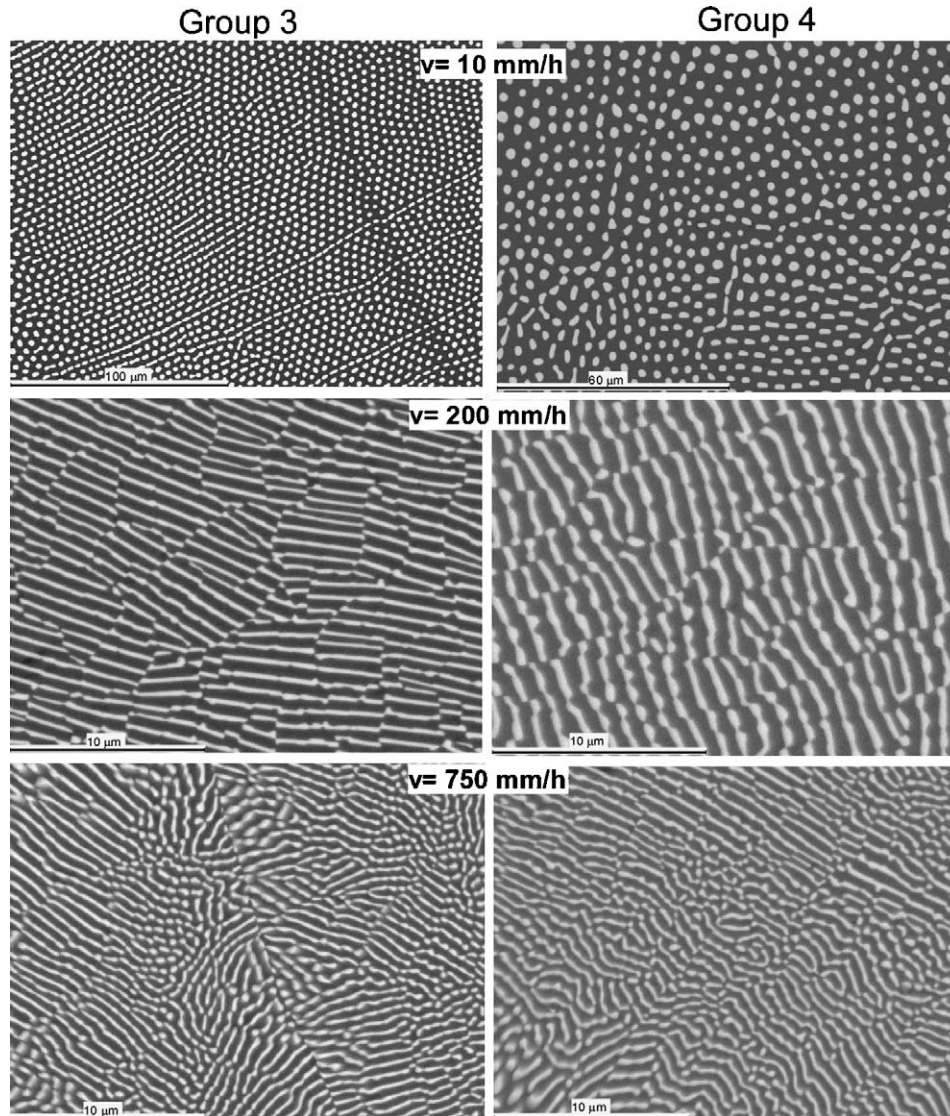


Fig. 7. Electron micrograph of the microstructures corresponding to the off-eutectic compositions For the  $\text{CeO}_2\text{:CoO}$  system.

At present, the lack in the literature of detailed microscopical studies on the effect of the growth rate on the eutectic microstructure prevents us from making clear statements but the observation that there exists a phase segregation in the liquid for low growth rates could be a plausible explanation of this interesting effect. This observation is attractive enough to renew the interest in the study of eutectic microstructures from both the fundamental point of view and the potential applications that may benefit from a well known growth mechanisms and the resulting microstructures.

#### Acknowledgements

This work has been funded by the following Spanish projects MAT2009-14324-C02-01 and CIT-120000-2007-50 and the European project ENSEMBLE NMP4-2008-213669. Saint Gobain-CREE (Cavaillon, France) is also acknowledged for funding.

#### References

1. Llorca J, Orera VM. Directionally solidified eutectic oxides. *Prog Mater Sci* 2006;**51**:711–809.
2. Waku Y, Sakuma T. Dislocation mechanism of deformation and strength of  $\text{Al}_2\text{O}_3\text{-YAG}$  single crystal composite at high temperatures above 1500 °C. *J Eur Ceram Soc* 2000;**20**:1453–8.
3. Oliete PB, Peña JI, Larrea A, Orera VM, Llorca J, Pastor JY, et al. Ultra-high-strength nanofibrillar  $\text{Al}_2\text{O}_3\text{-YAG-YSZ}$  eutectics. *Adv Mater* 2007;**19**:2313–8.
4. Merino RI, Peña JI, Larrea A, de la Fuente GF, Orera VM. Melt grown composite ceramics obtained by directional solidification: structural and functional applications. *Recent Res Dev Mater Sci* 2003;**4**:1–24.
5. Galasso FS. Unidirectionally solidified eutectics for optical, electronic and magnetic applications. *J Met* 1967;**19**:17–21.
6. Orera VM, Peña JI, Merino RI, Lázaro JA, Vallés JA, Rebolledo MA. Prospects of new planar optical waveguides based on eutectic microcomposites of insulating crystals: the  $\text{ZrO}_2\text{(c)-CaZrO}_3$  erbium doped system. *Appl Phys Lett* 1997;**71**:2746–8.
7. Revcolevschi A, Dhalenne G. Crystallographically aligned metal–oxide composite made by reduction of directionally solidified oxide–oxide eutectics. *Nature* 1985;**316**:335–6.

8. Revcolevschi A, Dhalenne G. Engineering oxide–oxide and metal–oxide microstructures in directionally solidified eutectics. *Adv Mater* 1993;**5**(9):657–62.
9. Sun C, Stimming U. Recent anode advances in solid oxide fuel cells. *J Power Sources* 2007;**171**:247–60.
10. Minh Q. Solid oxide fuel cell technology-features and applications. *Solid State Ionics* 2004;**174**:271–7.
11. Singhal SC, Kendall K. *High Temperature Solid Oxide Fuel Cells: Fundamental, Design and Applications*. Oxford: Elsevier; 2003.
12. Iwata T. Characterization of Ni–YSZ anode degradation for substrate-type solid oxide fuel cells. *J Electrochem Soc* 1996;**143**:1521–5.
13. Laguna-Bercero MA, Larrea A, Peña JI, Merino RI, Orera VM. Structured porous Ni– and Co–YSZ cermets fabricated from directionally solidified eutectic composites. *J Eur Ceram Soc* 2005;**25**:1455–62.
14. Laguna-Bercero MA, Larrea A, Peña JI, Merino RI, Orera VM. Crystallography and thermal stability of textured Co–YSZ cermets from eutectic precursors. *J Eur Ceram Soc* 2008;**28**:2325–9.
15. Laguna-Bercero MA, Larrea A, Merino RI, Peña JI, Orera VM. Stability of channeled Ni–YSZ cermets produced from self-assembled NiO–YSZ directionally solidified eutectics. *J Am Ceram Soc* 2005;**88**:3215–7; Larrea A, Laguna-Bercero MA, Peña JI, Merino RI, Orera VM. Structured porous Ni– and Co–YSZ cermets fabricated from directionally solidified eutectic composites. *Cent Eur J Phys* 2009;**7**:242–50.
16. Steele BCH. Appraisal of  $Ce_{1-y}Gd_yO_{2-y/2}$  electrolytes for IT-SOFC operation at 500 °C. *Solid State Ionics* 2000;**129**:95–110.
17. Peña JI, Merino RI, de la Fuente GF, Orera VM. Aligned  $ZrO_2(c)$ – $CaZrO_3$  eutectics grown by the laser floating zone method: electrical and optical properties. *Adv Mater* 1996;**8**:909–12.
18. Gil V, Moure C, Tartaj J. Sinterability, microstructures and electrical properties of Ni/Gd-doped ceria cermets used as anode materials for SOFCs. *J Eur Ceram Soc* 2007;**27**:4205–9.
19. Chen M, Hallstedt B, Grundy AN, Gauckler LJ.  $CoO_2$ – $CoO$  phase diagram. *J Am Ceram Soc* 2003;**86**:1567–70.
20. Hogan LM, Kraft RW, Lemkey FD. Eutectic grains. *Adv Mater Res* 1971;**5**:83–216.
21. Sayir A, Farmer SC. The effect of the microstructure on mechanical properties of directionally solidified  $Al_2O_3/ZrO_2(Y_2O_3)$  eutectic. *Acta Mater* 2000;**48**:4691–7.
22. Ashbrook RL. Directionally solidified ceramic eutectics. *J Am Ceram Soc* 1977;**60**:428–35.
23. Jackson KA, Hunt JD. Lamellar and rod eutectic growth. *Trans Metall Soc AIME* 1966;**236**:1129–42.
24. Orera VM, Larrea A. NaCl-assisted growth of micrometer-wide long single crystalline fluoride fibres. *Opt Mater* 2005;**27**:1726–9.
25. Larrea A, Orera VM. Porous crystal structures obtained from directionally solidified eutectic precursors. *J Cryst Growth* 2007;**300**:387–93.
26. Laguna-Bercero MA, Larrea A. YSZ-induced crystallographic reorientation of Ni particles in Ni–YSZ cermets. *J Am Ceram Soc* 2007;**90**:2954–60.
27. Ortega-San-Martin L, Peña JI, Larrea A, Gil V, Orera VM. Textured cermets of  $CeO_2$  (or GDC) with Co for solid oxide fuel cells anodes. *Int J Hydrogen Energy* 2010, doi:10.1016/j.ijhydene.2010.05.013.
28. Chadwick GA. Eutectic alloy solidification. *Prog Mater Sci* 1963–1965;**12**:99–182.
29. Minford WJ, Bradt RC, Stubican VS. Crystallography and microstructure of directionally solidified oxide eutectics. *J Am Ceram Soc* 1979;**62**:154–7.
30. Hunt JD, Chilton JP. Lamella → rod transition in binary eutectics. *J Inst Met* 1963;**91**:338–42.
31. Peña JI, Merino RI, Harlan NR, Larrea A, de la Fuente GF, Orera VM. Microstructure of  $Y_2O_3$  doped  $Al_2O_3$ – $ZrO_2$  eutectics grown by the laser floating zone method. *J Eur Ceram Soc* 2002;**22**:2595.
32. Merino RI, Peña JI, Orera VM. Compositionally graded YSZ–NiO composites by surface laser melting. *J Eur Ceram Soc* 2010;**30**:147–52.
33. Kennard FL, Bradt RC, Stubican VS. Eutectic solidification of  $MgO$ – $MgAl_2O_4$ . *J Am Ceram Soc* 1973;**56**:566–9.
34. Street KN, John St, Piatti G CF. The structures of unidirectionally solidified binary eutectics Al– $Al_4Ca$ , Al– $Al_4Ce$  and Al– $Al_3Y$ . *J Inst Met* 1967;**95**:326–32.
35. Savas MA, Smith RW. The structural degradation and lamellar to rod transition in the Bi–Cd eutectic during unidirectional growth. *J Mater Sci* 1985;**20**:881–8.
36. Yoshida M, Tsujimura T, Tsukagoshi T, Nakae H. Rod–lamella transition in directionally solidified Ni–W eutectic alloy. *J Jpn Inst Met* 1996;**60**:482–9 [in Japanese].